Article

Discovery Medicine 2026; 38(209): 1732–1743
https://doi.org/10.24976/Discov.Med.202638209.135

Beyond Morphology: A Nomogram Integrating CT Net Arterial Enhancement and Serum Biomarkers for Preoperative N-Staging in Colorectal Cancer

Yinghong Zhou[1], Wanglin Bao[1,*]

[1]Radiology Department, Wuyi First People's Hospital, 321200 Jinhua, Zhejiang, China
*Correspondence: 13758908925@139.com (Wanglin Bao)
Submitted: 11 March 2026 Revised: 20 April 2026 Accepted: 22 May 2026 Published: 20 June 2026

Background: Accurate preoperative assessment of lymph node (LN) metastasis dictates treatment strategies in colorectal cancer (CRC), yet traditional morphological criteria (e.g., size) lack sensitivity. We aimed to develop a diagnostic nomogram integrating functional hemodynamics and serum biomarkers to overcome these limitations.

Methods: Data from 130 CRC patients undergoing radical resection were retrospectively analyzed. Preoperative multi-phase computed tomography (CT) features, specifically Net Arterial Enhancement (△A) and morphological metrics, along with serum carcinoembryonic antigen (CEA) and carbohydrate antigen 19-9 (CA19-9) levels, were evaluated. A diagnostic nomogram was constructed based on multivariate logistic regression, with performance assessed using Area Under the Curve (AUC), bootstrap validation, and Decision Curve Analysis (DCA).

Results: Multivariate analysis revealed that traditional morphological features (size, shape, margin) were not independent predictors of metastasis. In contrast, △A ($p = 0.001$), CEA ($p < 0.001$), and CA19-9 ($p = 0.024$) were identified as significant independent predictors. The novel nomogram integrating these three variables achieved an AUC of 0.925 (95% CI 0.877–0.972), significantly outperforming both the conventional CT model incorporating short-axis diameter, short/long axis ratio, and △A (AUC 0.778, 95% CI 0.699–0.857; $p < 0.001$) and a pure morphology model combining short-axis diameter, short/long axis ratio, and margin status (AUC 0.734, 95% CI 0.649–0.819; $p < 0.001$). The model demonstrated excellent calibration (bias-corrected C-index: 0.917) and provided superior clinical net benefit across a wide range of threshold probabilities compared to standard strategies.

Conclusion: Within an integrated multivariable framework, functional hemodynamic parameters (△A) and biological markers offer preoperative predictive information that is not fully captured by size-based criteria alone, supporting their complementary role in nodal assessment. This nomogram provides a non-invasive and quantitative tool for patient-level preoperative N-staging based on index-node imaging surrogates, facilitating personalized surgical decision-making. Given that the model was developed in a modest single-center retrospective cohort and evaluated only through internal bootstrap validation, external validation in independent, preferably prospective, multi-center cohorts is required before the nomogram can be considered robust or adopted in routine clinical practice.

Keywords: colorectal cancer; lymph node metastasis; nomogram; hemodynamics; X-ray computed tomography; biomarkers; tumor

Introduction

Colorectal cancer (CRC) remains one of the most prevalent malignancies globally and a leading cause of cancer-related mortality [1,2]. Accurate preoperative assessment of regional lymph node (LN) metastasis, which dictates the clinical N-stage, is fundamentally critical for determining the optimal therapeutic strategy [3–5]. In clinical practice, the confirmed presence of LN metastasis not only guides the extent of surgical resection, such as the necessity for extended lymphadenectomy or total mesorectal excision (TME) in rectal cancers, but also serves as a primary indication for neoadjuvant [6,7]. Conversely, overestimation of LN involvement can subject patients to unwarranted surgical morbidity, prolonged postoperative recovery, and the toxicities associated with overtreatment [8]. Therefore, developing a highly accurate, non-invasive preoperative prediction tool is of paramount importance to tailor personalized oncology regimens and improve survival outcomes.

Currently, multi-detector computed tomography (MDCT) remains the cornerstone imaging modality for the preoperative staging of CRC [9]. Routine radiological evaluation predominantly relies on morphological and size-based criteria, such as the short-axis diameter (SAD), shape ratio, and margin contour, to differentiate metastatic from benign nodes [10,11]. However, this morphology-centric paradigm is fraught with diagnostic uncertainty. Extensive clinical literature indicates that relying solely on size criteria yields suboptimal sensitivity and specificity,

often failing to exceed 70% [12]. The fundamental flaw of this approach lies in the complex biological reality of tumor progression: enlarged lymph nodes frequently result from benign reactive hyperplasia secondary to tumor-induced inflammation, whereas morphologically normal-sized nodes may already harbor microscopic metastases [13,14]. This discrepancy highlights a critical clinical gap, necessitating a paradigm shift from purely anatomical measurements to functional and biological characterization.

To bridge this diagnostic gap, integrating functional imaging parameters with systemic tumor biomarkers offers a robust scientific avenue. Tumor-induced angiogenesis is a well-established hallmark of metastasis [15]. As CRC cells colonize regional lymph nodes, they stimulate the formation of a chaotic, hyperpermeable microvascular network to sustain their metabolic demands [16]. Multi-phase contrast-enhanced CT provides a non-invasive window into these profound hemodynamic alterations [17]. Specifically, net arterial enhancement (ΔA), quantifying the absolute increase in CT attenuation during the arterial phase relative to the unenhanced phase, serves as a macroscopic surrogate for tumor hypervascularity and microvessel density [18]. Unlike anatomical size, which changes slowly and unreliably, altered hemodynamics and hyperperfusion often precede macroscopic morphological enlargement, offering an earlier and more specific indicator of metastatic infiltration [19].

Concurrently, systemic serum biomarkers directly reflect the biological tumor burden and its invasive phenotype [20]. Carcinoembryonic antigen (CEA) and carbohydrate antigen 19-9 (CA19-9) are widely validated, standard-of-care glycoproteins involved in intercellular adhesion and metastatic dissemination in gastrointestinal tumors [21]. While individually these markers may lack the spatial specificity required for precise LN staging, their integration with localized functional imaging parameters can synergistically capture both the systemic biological aggressiveness and the regional pathophysiological changes of the tumor [22]. We hypothesize that a multidimensional approach combining local hemodynamic functional imaging (ΔA) with systemic biological markers (CEA, CA19-9) will inherently overcome the limitations of traditional anatomical measurements.

Therefore, this study aimed to develop and internally validate a quantitative diagnostic nomogram that integrates multi-phase CT hemodynamic parameters and routine preoperative serum biomarkers. By shifting the diagnostic focus from subjective morphological assessment to objective functional and biological quantification, we sought to provide clinicians with a robust, reproducible, and easily implementable tool for the precise preoperative prediction of lymph node metastasis in patients with colorectal cancer.

Methods

Study Design and Population

The study was approved by the Ethics Committee of Wuyi First People's Hospital (approval number: 2026-03-02), and all procedures adhered to the principles outlined in the Declaration of Helsinki. Due to the retrospective design and the use of anonymized clinical data, the requirement for informed consent was waived by the ethics committee.

Patients with pathologically confirmed CRC who underwent radical resection between January 2023 and February 2026 were screened for eligibility. The inclusion criteria were as follows: (1) pathologically confirmed colorectal adenocarcinoma; (2) availability of complete preoperative multi-phase contrast-enhanced CT images and serum tumor marker data (CEA, CA19-9) within two weeks prior to surgery; and (3) standard radical resection with regional lymph node dissection performed.

Patients were excluded if they: (1) received preoperative neoadjuvant radiochemotherapy, which could alter lymph node status and imaging features; (2) had distant metastasis (M1 stage) confirmed by imaging or exploration; (3) had a history of other malignancies; or (4) had poor CT image quality due to artifacts affecting quantitative measurement. Finally, a total of 130 patients were included in the analysis.

Image Acquisition Protocol

All patients underwent abdominal and pelvic CT scans using a 128-slice multi-detector CT scanner (Revolution EVO, GE Healthcare, Waukesha, WI, USA; SOMATOM Definition AS+, Siemens Healthineers, Erlangen, Bavaria, Germany). The scanning parameters were standardized as follows: tube voltage, 120 kVp; tube current, automatic exposure control; slice thickness, 5 mm; and reconstruction interval, 5 mm.

After non-enhanced scanning, a non-ionic iodinated contrast agent (Iohexol, 350 mgI/mL; Yangtze River Pharmaceutical Group, Taizhou, China) was injected intravenously at a rate of 3.0 mL/s (1.5 mL/kg body weight), followed by a 20-mL saline flush. Multi-phase imaging was triggered using a bolus-tracking technique. The arterial phase (AP) and venous phase (VP) were acquired at approximately 25–30 seconds and 60–70 seconds after injection, respectively.

Radiologic Feature Analysis

Two radiologists with more than 10 years of experience in abdominal imaging, who were blinded to the pathological N-stage and laboratory results, independently reviewed the CT images. Any discrepancies were resolved through consensus discussion. The largest regional lymph node in the drainage area of the tumor was selected as the target node for measurement. For patients with no visibly enlarged lymph nodes, the largest detectible node in the re-

gional lymphatic drainage area was measured. If multiple nodes of similar size were present, the one with the most suspicious features (e.g., largest SAD or highest density) was selected.

We acknowledge that the unit of radiologic analysis, a single target lymph node per patient, differs from the pathological reference standard, the patient-level N stage derived from the entire surgical specimen. We adopted this node-to-patient design for the following three reasons. Firstly, retrospective multi-phase CT datasets do not permit reliable one-to-one spatial co-registration between individual nodes on imaging and their corresponding histological counterparts after en bloc mesenteric or mesorectal resection, a limitation inherent to the majority of published CT- and MRI-based nodal staging studies. Additionally, clinical decisions, including the indication for neoadjuvant therapy and the extent of lymphadenectomy, are made at the patient level rather than the nodal level. A patient-level prediction model therefore has direct translational relevance. Furthermore, the largest or most morphologically suspicious node within the regional drainage territory is conventionally regarded as the "index node", most likely to reflect the metastatic status of the entire nodal basin, a convention consistent with prior CT- and MRI-based N-staging literature. Accordingly, all radiologic predictors in this study should be interpreted as index-node surrogates for patient-level nodal status, rather than as strictly node-specific measurements.

Quantitative measurements of CT attenuation were performed using a standardized Region of Interest (ROI) placement protocol. For each target lymph node, the ROI was manually drawn on the axial image slice displaying the maximum cross-sectional area. To minimize measurement bias, the ROI was maximized to cover approximately two-thirds to three-quarters of the nodal area, while strictly maintaining a margin of at least 1–2 mm from the nodal edge to avoid the partial volume effect from surrounding perinodal fat. Areas of cystic necrosis, coarse calcification, or artifacts were carefully excluded from the ROI to ensure the measurement reflected viable tumor tissue. To ensure consistency in hemodynamic assessment, the ROI position was electronically co-registered or carefully matched across the unenhanced, arterial, and venous phases on the same anatomical level. The mean attenuation value (in Hounsfield Units, HU) within the ROI was recorded for each phase.

Key morphological and hemodynamic parameters were defined as follows:

• Short-axis Diameter (SAD): The shortest diameter of the lymph node measured in the transverse plane.

• Shape Ratio: Calculated as the ratio of the short-axis diameter to the long-axis diameter (S/L ratio). A ratio closer to 1.0 indicates a rounder shape, suggesting malignancy.

• Net Arterial Enhancement (ΔA): Defined as the absolute increase in CT attenuation value during the arterial phase relative to the non-enhanced phase. The formula used was: $\Delta A = CT_{arterial} - CT_{plain}$. This parameter quantifies the hypervascularity of the lymph node, reflecting tumor-induced angiogenesis.

• Margin Status: Categorized as smooth (well-defined border) or irregular (spiculated or indistinct border).

To assess inter-observer variability, a subset of 30 patients was randomly selected and re-evaluated by a second radiologist, blinded to the clinical information and the first radiologist's measurements. The inter-observer agreement for continuous variables (SAD, net arterial enhancement) was evaluated using the Intraclass Correlation Coefficient (ICC), and for categorical variables (margin status) using Cohen's Kappa coefficient.

Clinical and Pathological Variables

Baseline demographic data (age, gender) and clinical characteristics (tumor location) were collected from electronic medical records. Preoperative serum levels of carcinoembryonic antigen (CEA) and carbohydrate antigen 19-9 (CA19-9) were measured within 14 days before surgery using electrochemiluminescence immunoassay (ECLIA) kits (CEA: Elecsys® CEA; CA19-9: Elecsys® CA19-9; Roche Diagnostics GmbH, Mannheim, Germany). All assays were performed in accordance with the manufacturer's instructions and routine laboratory quality-control procedures.

The histopathological N-stage was determined according to the 8th edition of the AJCC/UICC TNM staging system [23]. Patients were classified into a non-metastatic group (pN0 stage) and a metastatic group (pN+, comprising pN1 and pN2 categories) based on the final pathology report.

Statistical Analysis

All statistical analyses were performed using R software (version 4.5.2; The R Foundation for Statistical Computing, Vienna, Austria).

Continuous variables were tested for normality using the Shapiro-Wilk test. As all continuous variables examined in this study deviated significantly from a normal distribution, they were uniformly summarized as median [interquartile range, IQR] and compared between groups using the Mann-Whitney U test. Categorical variables were presented as frequencies (percentages) and compared using the Chi-square test or Fisher's exact test, as appropriate.

Model Construction and Validation

Univariate logistic regression analysis was performed to identify significant predictors of lymph node metastasis. Before multivariate modeling, a multicollinearity diagnosis was conducted for all candidate variables using the Variance Inflation Factor (VIF). A VIF value of >5 was considered indicative of severe multicollinearity. Variables with a p-value < 0.1 in the univariate analysis were entered

into a multivariate logistic regression model using a backward stepwise selection method based on the Akaike Information Criterion (AIC). To clearly delineate the incremental contribution of each category of predictor and to avoid conceptual overlap between morphological and functional domains, three models were constructed:

• Model 1, Morphological Model: Incorporating only conventional morphological features (short-axis diameter, short/long axis ratio, and margin status). This model represents the classical size- and shape-based paradigm of radiologic nodal assessment.

• Model 2, Conventional CT Model: Incorporating short-axis diameter, short/long axis ratio, and net arterial enhancement (ΔA). This model represents the commonly adopted size-shape-plus-enhancement paradigm in routine multi-phase CT interpretation. Margin status is intentionally excluded from Model 2 because its contribution is already captured in Model 1 (the purely morphological model). This specification allows the Model 1 vs Model 2 comparison to isolate the incremental value of ΔA beyond size and shape alone.

• Model 3, Combined Model: Incorporating the independent predictors identified by multivariate analysis, including ΔA, CEA, and CA19-9, representing the proposed integrated functional and biological paradigm.

The incremental discriminative value across the three models was compared using pairwise DeLong tests, thereby isolating the gain attributable to adding functional hemodynamic information to pure morphology (from Model 1 to Model 2), and the gain attributable to further integrating systemic biological markers (from Model 2 to Model 3).

The discrimination performance of the models was evaluated using the Receiver Operating Characteristic (ROC) curve and the Area Under the Curve (AUC). The DeLong test was used to compare the AUCs of the two models to determine the incremental value of the combined approach.

Based on the Combined Model, a quantitative nomogram was constructed using the rms package (version 7.0-0) in R. To evaluate the predictive accuracy and robustness of the established nomogram, internal validation was performed using a bootstrap resampling method with 1000 iterations. This resampling technique is particularly critical for mitigating the risk of overfitting and estimating the expected optimism in cohorts with modest sample sizes. The discriminative ability of the model was quantified using Harrell's concordance index (C-index), and a bias-corrected C-index was reported to reflect the model's generalized performance. Furthermore, model calibration, the degree of agreement between the nomogram-predicted probability of lymph node metastasis and the actual observed incidence, was visually assessed using a calibration curve derived from the resampled cohorts.

To translate the statistical performance of the nomogram into tangible clinical value, Decision Curve Analysis (DCA) was conducted using the dcurves package (version 0.5.0). While traditional metrics like the Area Under the Curve (AUC) evaluate diagnostic accuracy, DCA specifically quantifies the clinical net benefit across a continuous spectrum of threshold probabilities. The net benefit was calculated by subtracting the proportion of false positives from the proportion of true positives, weighted according to the relative harm of false-positive and false-negative results. In this study, the clinical utility of our novel combined nomogram was compared with the Conventional CT Model, as well as the default baseline strategies of "treat-all" (assuming all patients have metastasis) and "treat-none" (assuming no metastasis), thereby identifying the optimal threshold range for clinical decision-making.

Results

Baseline Demographic and Clinicopathologic Characteristics

A total of 130 patients with colorectal cancer were included in this study, comprising 73 patients (56.2%) in the non-metastatic group (pN0) and 57 patients (43.8%) in the metastatic group (pN+). The baseline characteristics of the study cohort are summarized in Table 1. There were no statistically significant differences between the two groups regarding age ($Z = -0.998$, $p = 0.319$), gender distribution ($\chi^2 = 0.060$, $p = 0.806$), or primary tumor location ($\chi^2 = 0.968$, $p = 0.915$), indicating a well-balanced study population.

In contrast, significant differences were observed in both serum biomarkers and CT radiologic features. Patients with lymph node metastasis exhibited significantly higher levels of preoperative serum CEA (median: 11.3 vs. 2.6 ng/mL, $Z = -6.742$, $p < 0.001$) and CA19-9 (median: 19.6 vs. 11.3 U/mL, $Z = -4.258$, $p < 0.001$). Regarding morphological features, metastatic lymph nodes presented with larger short-axis diameters (median: 9.6 vs. 8.0 mm, $Z = -4.200$, $p < 0.001$) and a rounder shape, as indicated by a higher short/long axis ratio (median: 0.80 vs. 0.73, $Z = -2.800$, $p = 0.005$). Notably, the hemodynamic parameter, the net arterial enhancement, was significantly higher in the pN+ group (median: 35 HU) compared to the pN0 group (median: 26 HU) ($Z = -5.317$, $p < 0.001$), reflecting the hypervascular nature of metastatic nodes.

Inter-Observer Agreement and Multicollinearity Assessment

To ensure the reliability of the radiologic measurements, inter-observer agreement was assessed in a randomly selected subset of patients. The reproducibility of quantitative measurements was excellent, with an intraclass correlation coefficient (ICC) of 0.989 (95% CI: 0.984–0.992) for short-axis diameter and 0.984 (95% CI: 0.977–

Table 1. Baseline demographic, clinical, and radiologic characteristics of the study population stratified by lymph node metastasis status.

Variable	Non-Metastatic (pN0) (N = 73)	Metastasis (pN+) (N = 57)	Statistic	*p*-value
Age (years), median [IQR]	63.0 [57.0, 69.0]	63.0 [59.0, 73.0]	Z = −0.998	0.319
Gender, n (%)			χ^2 = 0.060	0.806
Female	33 (45.2%)	27 (47.4%)		
Male	40 (54.8%)	30 (52.6%)		
Tumor Location, n (%)			χ^2 = 0.968	0.915
Ascending	18 (24.7%)	13 (22.8%)		
Descending	12 (16.4%)	8 (14.0%)		
Rectum	17 (23.3%)	16 (28.1%)		
Sigmoid	17 (23.3%)	11 (19.3%)		
Transverse	9 (12.3%)	9 (15.8%)		
CEA (ng/mL), median [IQR]	2.6 [1.7, 4.0]	11.3 [6.8, 16.0]	Z = −6.742	<0.001
CA19-9 (U/mL), median [IQR]	11.3 [7.3, 21.2]	19.6 [14.5, 30.0]	Z = −4.258	<0.001
LN Short-axis Diameter (mm), median [IQR]	8.0 [6.6, 9.2]	9.6 [7.9, 10.6]	Z = −4.200	<0.001
Short/Long Axis Ratio, median [IQR]	0.73 [0.67, 0.82]	0.80 [0.72, 0.86]	Z = −2.800	0.005
Net Arterial Enhancement (HU), median [IQR]	26 [18, 32]	35 [28, 43]	Z = −5.317	<0.001
LN Margin, n (%)			χ^2 = 11.245	<0.001
Irregular	31 (42.5%)	41 (71.9%)		
Smooth	42 (57.5%)	16 (28.1%)		

Note: Continuous variables, all of which deviated from a normal distribution based on the Shapiro-Wilk test, were presented as median [interquartile range, IQR] and compared between groups using the Mann-Whitney U test (reported as tie-corrected Z statistics based on the normal approximation). Categorical variables were presented as frequencies (percentages) and compared using Pearson's Chi-square test (reported as χ^2 statistics) without continuity correction. A two-sided p-value < 0.05 was considered statistically significant. Abbreviations: pN0, pathologically node-negative group; pN+, pathologically node-positive group (comprising pN1 and pN2 categories); CEA, carcinoembryonic antigen; CA19-9, carbohydrate antigen 19-9; LN, lymph node; HU, Hounsfield unit.

0.988) for net arterial enhancement. For the qualitative evaluation of margin status, the agreement between the two radiologists was substantial, yielding a Kappa value of 0.907 ($p < 0.001$).

Furthermore, prior to multivariate modeling, a collinearity diagnosis was performed to rule out redundancy among predictors. The variance inflation factors (VIF) for all candidate variables ranged from 1.10 to 2.82, which were well below the threshold of 5, indicating no severe multicollinearity among the imaging and clinical parameters included in the analysis (Table 2).

Table 2. Collinearity diagnosis of candidate predictors using variance inflation factors (VIF).

Variable	VIF
Short-axis Diameter (mm)	1.89
Net Arterial Enhancement (HU)	2.75
Short/Long Axis Ratio	2.82
CEA (ng/mL)	1.17
CA19-9 (U/mL)	1.10
Margin Status (Irregular)	2.38

Note: A VIF value <5 indicates no severe multicollinearity. Abbreviations: VIF, Variance Inflation Factor; CEA, carcinoembryonic antigen; CA19-9, carbohydrate antigen 19-9; HU, Hounsfield unit.

Predictors of Lymph Node Metastasis and Model Construction

Univariate logistic regression analysis identified several significant predictors of lymph node metastasis (Table 3). Specifically, morphological features, such as larger short-axis diameter (odds ratio [OR] = 1.56, 95% confidence interval [CI]: 1.26–1.94, $p < 0.001$), irregular margin status (OR = 3.47, 95% CI: 1.65–7.28, $p < 0.001$), and a rounder shape (Short/Long axis ratio per 0.1-unit increase: OR = 1.64, 95% CI: 1.16–2.31, $p = 0.005$), were associated with an increased risk of metastasis. Additionally, hemodynamic parameters and serum biomarkers showed strong predictive value.

To adjust for confounding factors and identify independent predictors, a multivariate logistic regression analysis was performed using a stepwise selection method. Interestingly, traditional morphological features (size, shape, and margin) were not retained in the final model. Instead, the analysis identified Net Arterial Enhancement (OR = 1.09, 95% CI: 1.04–1.16, $p = 0.001$), CEA (OR = 1.41, 95% CI: 1.23–1.62, $p < 0.001$), and CA19-9 (OR = 1.04, 95% CI: 1.01–1.08, $p = 0.024$) as the three independent predictors of lymph node metastasis. This finding indicates that,

Table 3. Univariate and multivariate logistic regression analysis of predictors for lymph node metastasis.

Variable	Univariate OR (95% CI)	*p* value	Multivariate OR (95% CI)	Adj. *p* value
Short-axis diameter (mm)	1.56 (1.26–1.94)	<0.001	-	-
Net arterial enhancement (HU)	1.10 (1.06–1.15)	<0.001	1.09 (1.04–1.16)	0.001
Short/long axis ratio (per 0.1 unit)	1.64 (1.16–2.31)	0.005	-	-
CEA (ng/mL)	1.46 (1.28–1.67)	<0.001	1.41 (1.23–1.62)	<0.001
CA19-9 (U/mL)	1.05 (1.02–1.08)	<0.001	1.04 (1.01–1.08)	0.024
Margin status (Irregular)	3.47 (1.65–7.28)	<0.001	-	-

Note: The Odds Ratio for Short/Long Axis Ratio is calculated per 0.1-unit increment. Variables included in the multivariate analysis were selected based on a *p*-value < 0.1 in the univariate analysis and finalized using stepwise selection based on AIC. Dash (-) indicates variables not retained in the final multivariate model during stepwise selection. Abbreviations: CI, Confidence Interval; OR, Odds Ratio; HU, Hounsfield Unit.

once ΔA and the serum biomarkers are jointly accounted for, the morphological variables no longer provide additional independent predictive information in this cohort. It should not be interpreted as evidence that morphological features are clinically irrelevant. Rather, their diagnostic signal appears to overlap substantially with that of the retained functional and biological predictors.

Diagnostic Performance and Incremental Value

To dissect the incremental diagnostic value contributed by each conceptual domain, including morphology, functional hemodynamics, and systemic biology, three hierarchical models were constructed and compared. The Receiver Operating Characteristic (ROC) curves for all three models are presented in Fig. 1. The Morphological model (Model 1), comprising short-axis diameter, shape ratio, and margin status, yielded a modest discriminative performance with an Area Under the Curve (AUC) of 0.734 (95% CI: 0.649–0.819), reflecting the well-recognized limitations of size- and contour-based criteria alone. The Conventional CT Model (Model 2), which combined short-axis diameter, short/long axis ratio, and net arterial enhancement (ΔA), yielded an AUC of 0.778 (95% CI: 0.699–0.857). Notably, pairwise DeLong testing indicated that the incremental improvement achieved by adding ΔA to the pure morphology model did not reach statistical significance (ΔAUC = 0.044, $p = 0.161$). This finding suggests that, within an exclusively CT-based framework, functional hemodynamic information alone yields only a limited and statistically non-significant improvement over morphological assessment. In contrast, the New Combined Model (Model 3), integrating ΔA with the serum biomarkers CEA and CA19-9, demonstrated a substantial improvement in discrimination, achieving an AUC of 0.925 (95% CI: 0.877–0.972). This improvement was highly statistically significant relative to both comparator models (ΔAUC = 0.147 over Model 2, $p < 0.001$; ΔAUC = 0.191 over Model 1, $p < 0.001$).

These hierarchical comparisons reveal a clinically important pattern. Neither morphology alone nor morphology combined with intra-CT functional information is sufficient for accurate preoperative nodal assessment, whereas the integration of localized hemodynamic imaging with systemic biological markers produces a decisive and statistically significant leap in diagnostic performance. This decomposition clarifies the conceptual architecture of the proposed approach, from morphology to combined morphology-plus-function, to an integrated functional-biological paradigm, and supports Model 3 as the optimal framework for preoperative nodal risk stratification.

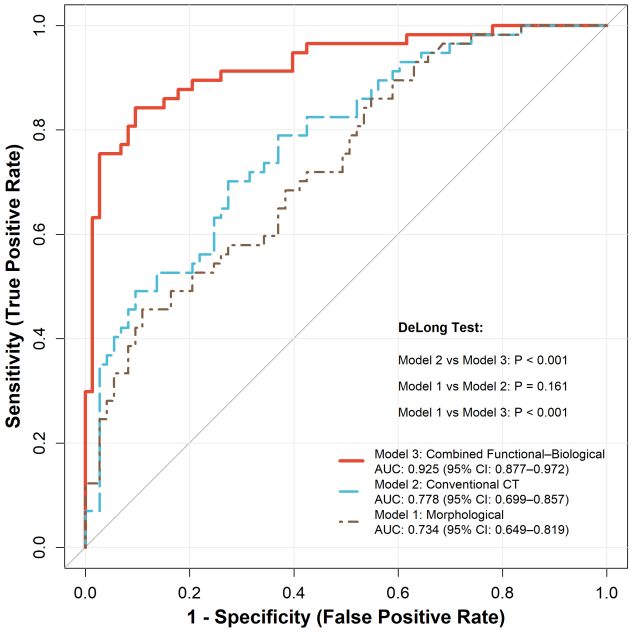

Fig. 1. Comparison of receiver operating characteristic (ROC) curves. The Morphological Model (Model 1; brown dot-dashed line) incorporated short-axis diameter, shape ratio, and margin status. The Conventional computed tomography (CT) Model (Model 2; blue long-dashed line) combined short-axis diameter, short/long axis ratio, and net arterial enhancement (ΔA). The Combined Functional-Biological Model (Model 3; red solid line) integrated ΔA with serum carcinoembryonic antigen (CEA) and carbohydrate antigen 19-9 (CA19-9).

At the Youden index-derived optimal cut-off values, the three models exhibited markedly different classification performance. The Morphological Model (Model 1) yielded an optimal cut-off of 0.618, corresponding to a sensitivity of 45.6% (95% CI 32.4%–59.3%) and a specificity of 89.0% (95% CI 79.5%–95.1%), indicating that size- and shape-based criteria alone missed more than half of the metastatic cases. The Conventional CT Model (Model 2), with an optimal cut-off of 0.423, achieved a more balanced but still modest performance (sensitivity 70.2%, 95% CI 56.6%–81.6%; specificity 72.6%, 95% CI 60.9%–82.4%). In contrast, the Combined Functional-Biological Model (Model 3), at an optimal cut-off of 0.373, produced the most favorable joint profile, with both sensitivity (84.2%, 95% CI 72.1%–92.5%) and specificity (90.4%, 95% CI 81.2%–96.1%) exceeding 80%, and a correspondingly higher Youden's J statistic (0.746) compared with Model 1 (0.347) and Model 2 (0.428).

Construction and Validation of the Nomogram

Based on the multivariate logistic regression analysis, a quantitative nomogram was developed to predict the individual probability of lymph node metastasis (Fig. 2). In this updated scoring system, net arterial enhancement, CEA, and CA19-9 were integrated to calculate the risk score, with net arterial enhancement and CEA identified as the strongest contributors.

Internal validation was performed using the bootstrap method with 1000 resamples to assess the model's stability. The bias-corrected C-index was 0.917, which was very close to the apparent C-index (0.925), indicating minimal overfitting and robust predictive power. The calibration curve (Fig. 3) demonstrated excellent agreement between the nomogram-predicted probabilities and the observed rates, with the bias-corrected curve adhering closely to the ideal 45-degree reference line.

Clinical Usefulness

Decision Curve Analysis (DCA) was conducted to evaluate the clinical utility of the nomogram (Fig. 4). The DCA demonstrated that using the New Combined Nomogram to predict lymph node metastasis provided a higher net benefit than either the "treat-all" or "treat-none" strategies across a wide range of threshold probabilities (approximately 10% to 85%). Crucially, the New Combined Nomogram consistently outperformed the Conventional CT Model throughout most of the probability range. This finding suggests that a decision-making strategy based on hemodynamic parameters and serum biomarkers is superior to relying on traditional morphological features, potentially preventing unnecessary lymph node dissections while ensuring high-risk patients are correctly identified.

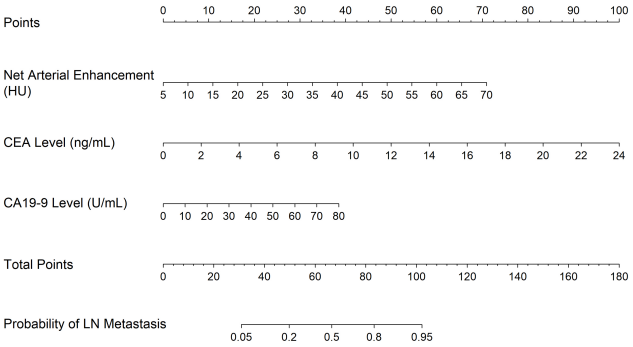

Fig. 2. Clinical-hemodynamic nomogram for preoperative prediction of lymph node metastasis. The nomogram incorporates three independent predictors: net arterial enhancement, CEA, and CA19-9. To use the nomogram, the value of each variable was located on its respective axis, and a vertical line was drawn upwards to the "Points" axis to assign a score. The scores for all variables were then summed, and the total score was located on the "Total Points" axis to determine the corresponding probability of metastasis.

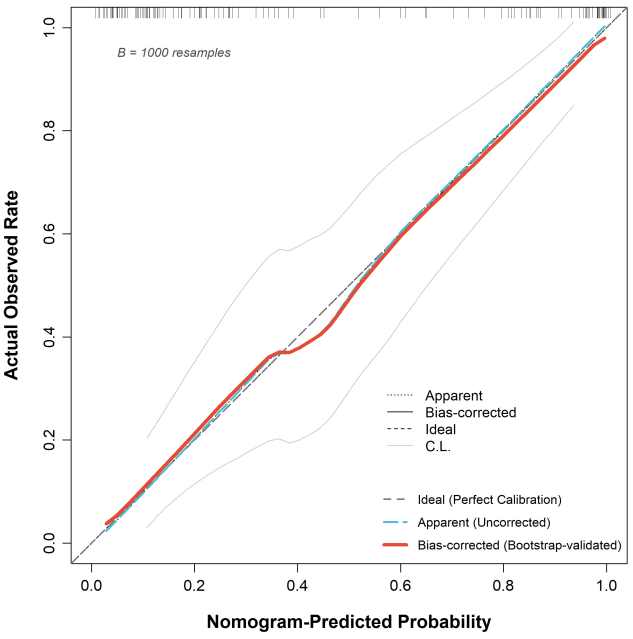

Fig. 3. Calibration curve of the nomogram. The x-axis represents the predicted probability of metastasis, and the y-axis represents the actual observed rate. The diagonal line represents perfect prediction, where predicted probabilities match observed rates.

Discussion

In this study, we developed and internally validated a novel, quantitative nomogram for the preoperative prediction of lymph node (LN) metastasis in patients with colorectal cancer (CRC). Through hierarchical comparison of three models—a pure morphological model, a conventional CT model that additionally incorporates net arterial enhance-

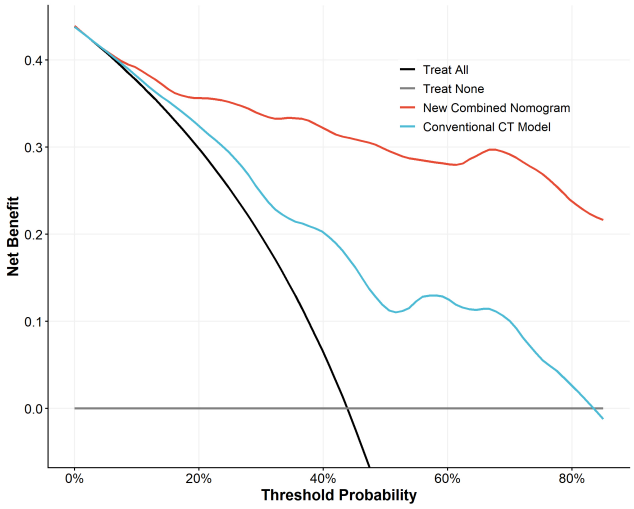

Fig. 4. Decision curve analysis (DCA). The y-axis measures the net benefit, and the x-axis represents the threshold probability. The New Combined Nomogram (red solid line), incorporating net arterial enhancement, CEA, and CA19-9, demonstrates the highest net benefit across a wide range of threshold probabilities. It consistently outperforms the Conventional CT Model (blue solid line). The gray lines represent the reference strategies of "Treat-all" and "Treat-none".

ment (ΔA), and a combined functional–biological model that further integrates serum CEA and CA19-9—we were able to delineate the distinct diagnostic contributions of morphology, functional hemodynamics, and systemic biology. The results revealed a clinically meaningful stepwise pattern. Morphology alone provided only modest discrimination, the addition of ΔA yielded a numerically higher but statistically non-significant increment, and only the further integration of systemic biomarkers produced a substantial and highly significant leap in performance. This decomposition addresses the conceptual architecture of our approach and demonstrates that the proposed paradigm shift does not rest on CT information alone, but rather on the synergistic integration of localized hemodynamic imaging with systemic biological signals.

An important observation from our multivariate analysis is that, when functional hemodynamic parameters and biological tumor markers were jointly considered, traditional morphological features, such as short-axis diameter, shape ratio, and margin status, were not retained as independent predictors of metastasis. This finding should be interpreted with appropriate caution rather than as evidence that morphological assessment is clinically obsolete. Several plausible explanations merit consideration. Morphological features and ΔA may share a substantial portion of the diagnostic signal, since enlarged and irregularly shaped nodes tend also to exhibit increased tumor-driven perfusion. The statistical power of a modest single-center cohort to detect small-to-moderate independent effects of multiple correlated morphological variables is limited, and stepwise AIC-based variable selection is known to be sensitive to sample size and model specification. Morphological assessment therefore remains the indispensable first step in radiological nodal evaluation and is what allows a target node to be identified in the first place.

The hierarchical model comparison adds a complementary quantitative perspective on this issue. Moving from pure morphology (Model 1) to a conventional CT assessment that additionally incorporates ΔA (Model 2) produced only a modest and statistically non-significant improvement in AUC. This observation warrants careful interpretation. It does not imply that ΔA, which emerged as an independent predictor in the multivariable analysis, is biologically uninformative. Rather, within an exclusively CT-based framework, functional hemodynamic information appears to be partially confounded by, and to share diagnostic signal with, coexisting morphological features. In other words, enlarging and more irregular nodes tend also to be hypervascular, so simply layering ΔA onto morphology does not substantially extend the intrinsic informational content of CT-only assessment. A more substantial and statistically significant improvement in AUC was observed only when ΔA was combined with systemic biomarkers reflecting tumor burden and invasiveness (CEA and CA19-9), with the AUC increasing from 0.778 to 0.925. Taken together, these hierarchical results suggest that improving preoperative N-staging in this cohort is unlikely to be achieved by adding further imaging descriptors alone, and that the integration of localized functional imaging with systemic biological information provides predictive value that complements, rather than replaces, conventional morphological assessment.

For decades, the short-axis diameter (SAD) has been the cornerstone of preoperative N-staging [24]. The prevailing logic assumes that metastatic deposits inevitably increase lymph node volume. However, a growing body of literature suggests that size alone, while informative, is an imperfect surrogate for metastatic status [25,26]. In our univariate analysis, while SAD was statistically associated with metastasis, it did not retain independent significance in the multivariate model once functional and biological predictors were included. Two concurrent biological phenomena likely contribute to this limited incremental value of size in the multivariable setting.

First, the phenomenon of "benign enlargement" often confounds diagnosis [27]. The primary tumor creates a local inflammatory microenvironment, leading to reactive lymphoid hyperplasia and sinus histiocytosis in the regional draining lymph nodes [28]. These benign immune responses can cause significant nodal enlargement, mimicking malignancy and leading to false positives (over-staging) [29]. Second, and perhaps more dangerously, is the issue of "microscopic metastasis" [30]. Early-stage metastatic infiltration often occurs without immediate gross anatomical

distortion [31]. Tumor clusters can colonize a lymph node while maintaining a normal SAD, typically <5 mm or <8 mm [26]. Consequently, a diagnostic strategy that relies solely on a size threshold (e.g., >10 mm) inherently lacks the sensitivity to detect these small but clinically significant metastases. Our findings corroborate the limitations of size criteria reported in previous studies, reinforcing the urgent need for biomarkers that transcend mere physical dimensions.

The superior predictive power of Net Arterial Enhancement (ΔA) in our model is not accidental; it is rooted in the fundamental pathophysiology of tumor angiogenesis. Metastasis is an angiogenesis-dependent process [32,33]. When CRC cells detach from the primary tumor and lodge in regional lymph nodes, their survival and proliferation depend on the induction of a new vascular supply [34]. These tumor-induced neovessels are structurally and functionally distinct from the mature vasculature of normal lymph nodes.

Normal lymph nodes typically exhibit a balanced, centrifugal blood supply with moderate enhancement [35]. In contrast, metastatic nodes are characterized by high microvessel density (MVD) and immature, leaky vessels lacking a complete basement membrane [36]. This "chaotic" vascular architecture leads to a rapid and intense wash-in of contrast agents during the arterial phase [37]. The parameter ΔA effectively captures this hypervascular physiological state. A higher ΔA value serves as a macroscopic radiologic surrogate for microscopic tumor angiogenesis [38]. Importantly, these hemodynamic changes often precede morphological enlargement. A metastatic node may still be small in size, but its "metabolic hunger", reflected by increased arterial perfusion, betrays its malignant nature [39]. By capturing this functional alteration, ΔA provides a complementary window into nodal status that, in our cohort, contributed independent predictive information beyond what was provided by morphological descriptors.

While ΔA provides specific regional information, LN metastasis is also a manifestation of the tumor's systemic biological aggressiveness [40]. This study highlights the independent predictive value of CEA and CA19-9. Carcinoembryonic antigen (CEA), an intercellular adhesion molecule, is integral to the mechanism of metastatic dissemination [41]. Elevated preoperative CEA levels correlate with a higher tumor burden and a propensity for lymphatic invasion [41]. Similarly, CA19-9, though more commonly associated with pancreaticobiliary malignancies, has shown prognostic relevance in CRC, particularly in mucinous adenocarcinomas [42].

Our results demonstrate a powerful synergy between imaging and biology. The combined nomogram integrates the "local functional view" (hemodynamic enhancement of the specific node) with the "systemic biological view" (serum tumor burden). This multi-dimensional approach minimizes the blind spots of using either modality in isolation. For instance, a patient with a small, equivocal lymph node might be accurately flagged as high-risk by our nomogram if they exhibit both high ΔA and elevated CEA, thereby preventing under-staging.

Statistical significance does not always translate to clinical utility. However, our Decision Curve Analysis (DCA) confirms that the proposed nomogram offers a tangible net benefit across a wide range of threshold probabilities (10% to 85%). This has profound implications for surgical planning.

In the context of locally advanced CRC, accurate identification of N-stage determines the necessity for neoadjuvant therapies [43]. For rectal cancer specifically, the decision to proceed with Total Mesorectal Excision (TME) versus a more limited resection, or the decision to administer preoperative chemoradiotherapy, hinges on N-status [43]. A "treat-all" strategy exposes pN0 patients to the toxicity of chemotherapy and radiation, while a "treat-none" strategy risks local recurrence in pN+ patients. Our nomogram provides a personalized risk score that can aid multidisciplinary teams (MDT) in navigating these complex decisions. For example, a high nomogram score might prompt a surgeon to perform a more extensive lymphadenectomy or suggest a radiologist revisit the scan for subtle signs of extra-nodal extension, thereby tailoring the treatment to the individual patient's risk profile.

Despite the promising results, this study is not without limitations. First, the retrospective design inherently introduces potential selection bias. Although we adhered to strict inclusion criteria, patients with incomplete clinical data were excluded, which may affect the generalizability of the findings. Most importantly, a methodological caveat must be acknowledged regarding the mismatch between the imaging unit of analysis and the pathological reference standard. Our radiologic measurements, including Net Arterial Enhancement (ΔA), short-axis diameter, shape ratio, and margin status, were performed on a single representative target node (the largest or most morphologically suspicious node in the regional drainage area) identified on preoperative CT. In contrast, the pathological endpoint was the patient-level N stage determined from the entire surgical specimen, which typically contained twelve or more dissected nodes per patient. Consequently, we cannot definitively confirm that the specific node measured on CT corresponds one-to-one to the histologically metastatic node(s) identified in the pathology report. This node-to-patient mismatch is an inherent limitation of retrospective CT-based nodal staging studies, because en bloc mesenteric or mesorectal resection precludes reliable spatial co-registration between individual imaging nodes and their histological counterparts. Several considerations partially mitigate, but do not eliminate, this concern. Biologically, regional lymphatic drainage within a common mesenteric territory is contiguous, and the hemodynamic milieu of the draining basin is shaped by the angiogenic activity of the

primary tumor. The ΔA of the index node may therefore serve as a macroscopic surrogate for the perfusion status of the entire nodal basin rather than a strictly node-specific measurement. Treatment decisions such as neoadjuvant therapy or extended lymphadenectomy are made at the patient level, aligning the unit of prediction with the unit of clinical action. Nevertheless, we explicitly caution that our findings should be interpreted as patient-level risk stratification based on an index-node imaging surrogate, rather than as direct node-by-node diagnostic accuracy. Future prospective studies employing *ex vivo* specimen CT, intraoperative node marking, or radio-pathological co-registration protocols are warranted to establish true node-level correspondence and to determine whether ΔA retains its predictive power at the individual nodal level. Also, our measurement of ΔA was based on a 2D Region of Interest (ROI) on the largest cross-section of the target node. While this is the standard clinical approach, it may not capture the heterogeneity of the entire lymph node volume. Future studies could explore 3D volumetric analysis or radiomics texture analysis, which might extract even more subtle features of intranodal heterogeneity that are invisible to the naked eye. Additionally, the integration of dual-energy CT (DECT) parameters, such as iodine concentration maps, could provide an even more direct quantification of blood volume, potentially further refining the accuracy of hemodynamic assessment.

A further and particularly important limitation concerns the generalizability and true robustness of the proposed nomogram. Our model was developed in a relatively modest single-center retrospective cohort of 130 patients, and its predictive performance was assessed only through internal bootstrap resampling with 1000 iterations. Although the bootstrap resampling yielded a bias-corrected C-index of 0.917, closely approximating the apparent C-index of 0.925 and suggesting minimal optimism within the development cohort, it is important to emphasize that internal bootstrap validation cannot substitute for independent external validation. Bootstrap resampling, by construction, draws repeatedly from the same underlying sample and is therefore unable to detect systematic biases related to the specific patient population, scanner vendor, contrast injection protocol, radiologist reading practice, or laboratory assay platform represented in our single-center cohort. Consequently, the high discrimination performance reported here (AUC 0.925) should be interpreted with caution and regarded as an upper-bound, best-case estimate obtained under training-set conditions, rather than as a guaranteed indicator of real-world performance. External validation in geographically and institutionally independent cohorts is therefore an essential prerequisite before the nomogram can be considered genuinely robust or translated into routine clinical practice.

Conclusion

In conclusion, this study demonstrates that, within an integrated multivariable framework, the combination of CT net arterial enhancement (ΔA), CEA, and CA19-9 provides preoperative predictive information for lymph node metastasis in colorectal cancer that extends beyond what is captured by morphological features alone. We have constructed and internally validated a clinical-hemodynamic nomogram based on these three independent predictors, which achieved favorable discrimination and clinical net benefit. Rather than replacing conventional morphological assessment, the proposed nomogram is intended to complement it by refining patient-level risk stratification, particularly in cases where morphology alone is equivocal. Importantly, these findings should be regarded as preliminary and hypothesis-generating. Prospective, multi-center external validation in independent cohorts with heterogeneous imaging platforms and clinical workflows is an essential prerequisite before the nomogram can be considered genuinely robust or translated into routine clinical practice.

Availability of Data and Materials

The data that support the findings of this study are available from the corresponding author upon reasonable request.

Author Contributions

YHZ and WLB designed the research study. YHZ performed the research. YHZ and WLB analyzed the data. WLB drafted the article. Both authors contributed to the important editorial changes in the manuscript. Both authors read and approved the final manuscript. Both authors have participated sufficiently in the work to take public responsibility for appropriate portions of the content and agreed to be accountable for all aspects of the work in ensuring that questions related to its accuracy or integrity.

Ethics Approval and Consent to Participate

The study was approved by the Ethics Committee of Wuyi First People's Hospital (approval number: 2026-03-02), and all procedures followed the principles of the Declaration of Helsinki. Due to the retrospective design and the use of anonymized clinical data, the requirement for informed consent was waived by the ethics committee.

Acknowledgment

Not applicable.

Funding

This research received no external funding.

Conflict of Interest

The authors declare no conflict of interest.

References

[1] Ji YT, Liu SW, Zhang YM, Duan HY, Liu XM, Feng ZW, *et al*. Comparison of the latest cancer statistics, cancer epidemic trends and determinants between China and the United States. Chinese Journal of Oncology. 2024; 46: 646–656. https://doi.org/10.3760/cma.j.cn112152-20240208-00068. (In Chinese)

[2] Zhang J, Ou D, Xie A, Chen D, Li X. Global burden and cross-country health inequalities of early-onset colorectal cancer and its risk factors from 1990 to 2021 and its projection until 2036. BMC Public Health. 2024; 24: 3124. https://doi.org/10.1186/s12889-024-20624-4.

[3] Shao F, Zhou Q, Yu F, Pan L, Li L. Clinical value of nano-carbon lymphatic tracer for regional lymph node dissections of rectal cancer after neoadjuvant chemoradiotherapy. Journal of Applied Clinical Medical Physics. 2024; 25: e14406. https://doi.org/10.1002/acm2.14406.

[4] Inoue H, Sasaki K, Nozawa H, Kawai K, Murono K, Emoto S, *et al*. Therapeutic significance of D3 dissection for low rectal cancer: a comparison of dissections between the lateral pelvic lymph nodes and the lymph nodes along the root of the inferior mesenteric artery in a multicenter retrospective cohort study. International Journal of Colorectal Disease. 2021; 36: 1263–1270. https://doi.org/10.1007/s00384-021-03858-1.

[5] Delclaux I, Ventre KS, Jones D, Lund AW. The tumor-draining lymph node as a reservoir for systemic immune surveillance. Trends in Cancer. 2024; 10: 28–37. https://doi.org/10.1016/j.trecan.2023.09.006.

[6] Miyakita H, Chan LF, Okada K, Kayano H, Mori M, Sadahiro S, *et al*. Predictors and histological effects of preoperative chemoradiotherapy for rectal cancer and control of lateral lymph node metastasis. BMC Gastroenterology. 2022; 22: 334. https://doi.org/10.1186/s12876-022-02414-7.

[7] Singhi AN, Lee TG, Ahn HM, Shin HR, Choi MJ, Jo MH, *et al*. Lymph node metastasis following chemoradiotherapy in advanced rectal cancer: ypT2-focused analyses of total mesorectal excision specimens. Techniques in Coloproctology. 2024; 29: 15. https://doi.org/10.1007/s10151-024-03046-7.

[8] Hou Z, Lin X, Dong B, Lin Z, Zhang Y, Liu X, *et al*. Overestimation of contralateral hilar lymph node metastasis in non-metastatic non-small cell lung cancer and its predictive model: HAM. Radiotherapy and Oncology. 2024; 201: 110575. https://doi.org/10.1016/j.radonc.2024.110575.

[9] Olsen ASF, Gundestrup AK, Kleif J, Thanon T, Bertelsen CA. Accuracy of preoperative staging with multidetector computed tomography in colon cancer. Colorectal Disease. 2021; 23: 680–688. https://doi.org/10.1111/codi.15415.

[10] Li S, Li Z, Wang L, Wu M, Chen X, He C, *et al*. CT morphological features for predicting the risk of lymph node metastasis in T1 colorectal cancer. European Radiology. 2023; 33: 6861–6871. https://doi.org/10.1007/s00330-023-09688-9.

[11] Alhanafy A, Abdullah MS, Hafez H, Abbas H. Non Size Based Morphology Criteria for Assessment of Response in Patients with Liver Metastases of Gastrointestinal Origin Receiving Systemic Treatment. Asian Pacific Journal of Cancer Prevention. 2018; 19: 1655–1660. https://doi.org/10.22034/APJCP.2018.19.6.1655.

[12] Bipat S, Glas AS, Slors FJM, Zwinderman AH, Bossuyt PMM, Stoker J. Rectal cancer: local staging and assessment of lymph node involvement with endoluminal US, CT, and MR imaging–a meta-analysis. Radiology. 2004; 232: 773–783. https://doi.org/10.1148/radiol.2323031368.

[13] Wang D, Hu Y, Zhan C, Zhang Q, Wu Y, Ai T. A nomogram based on radiomics signature and deep-learning signature for preoperative prediction of axillary lymph node metastasis in breast cancer. Frontiers in Oncology. 2022; 12: 940655. https://doi.org/10.3389/fonc.2022.940655.

[14] Lee T, Horvat N, Gollub MJ, Garcia-Aguilar J, Kim TH. Prognostic value of lateral lymph node metastasis in pretreatment MRI for rectal cancer in patients undergoing neoadjuvant chemoradiation followed by surgical resection without lateral lymph node dissection: A systemic review and meta-analysis. European Journal of Radiology. 2024; 178: 111601. https://doi.org/10.1016/j.ejrad.2024.111601.

[15] Hsu WH, LaBella KA, Lin Y, Xu P, Lee R, Hsieh CE, *et al*. Oncogenic KRAS Drives Lipofibrogenesis to Promote Angiogenesis and Colon Cancer Progression. Cancer Discovery. 2023; 13: 2652–2673. https://doi.org/10.1158/2159-8290.CD-22-1467.

[16] Lv Q, Wang Y, Xiong Z, Xue Y, Li J, Chen M, *et al*. Microvascularized tumor assembloids model for drug delivery evaluation in colorectal cancer-derived peritoneal metastasis. Acta Biomaterialia. 2023; 168: 346–360. https://doi.org/10.1016/j.actbio.2023.06.034.

[17] Zhao L, Zhou W, Fu Y, Ge Y, Feng L, Wang X, *et al*. Diagnostic value of one-stop CT energy spectrum and perfusion for angiogenesis in colon and rectum cancer. BMC Medical Imaging. 2024; 24: 116. https://doi.org/10.1186/s12880-024-01291-8.

[18] Yamamoto T, Gulanbar A, Hayashi K, Kohno A, Komai Y, Yonese J, *et al*. Is hypervascular papillary renal cell carcinoma present? Abdominal Radiology (New York). 2021; 46: 1687–1693. https://doi.org/10.1007/s00261-020-02809-8.

[19] Liu X, Yuan Y, Chen XL, Fang Z, Liu SY, Pu H, *et al*. Radiomics from dual-energy CT-derived iodine maps for predicting lymph node metastases in patients with resectable rectal cancer. Journal of X-ray Science and Technology. 2025; 33: 553–564. https://doi.org/10.1177/08953996241313322.

[20] Paku M, Uemura M, Kitakaze M, Miyoshi N, Takahashi H, Mizushima T, *et al*. Clinical Significance of Preoperative and Postoperative Serum CEA and Carbohydrate Antigen 19-9 Levels in Patients Undergoing Curative Resection of Locally Recurrent Rectal Cancer. Diseases of the Colon and Rectum. 2023; 66: 392–400. https://doi.org/10.1097/DCR.0000000000002655.

[21] Lee JO, Kim M, Lee JH, Kim Y, Lim HK, Kwon YH, *et al*. Carbohydrate antigen 19-9 plus carcinoembryonic antigen for prognosis in colorectal cancer: An observational study. Colorectal Disease. 2023; 25: 272–281. https://doi.org/10.1111/codi.16372.

[22] Ji HB, Qian B, Hu JJ, Qi W, Che ZG. Use of Dynamic Contrast-Enhanced Magnetic Resonance Imaging Combined With Serum Carcinoembryonic Antigen and Carbohydrate Antigen 19-9 in Predicting Colorectal Cancer Liver Metastasis. Journal of Clinical Ultrasound. 2025; 53: 612–619. https://doi.org/10.1002/jcu.23917.

[23] Weiser MR. AJCC 8th Edition: Colorectal Cancer. Annals of Surgical Oncology. 2018; 25: 1454–1455. https://doi.org/10.1245/s10434-018-6462-1.

[24] Zhou W, Dai J, Zheng K, Peng X, Zhang Y, Jiang C, *et al*. Comparison of [^{18}F]AlF-NOTA-FAPI-04 PET/CT and [^{18}F]FDG PET/CT for diagnosing lymph node metastasis in malignant tumors. Frontiers in Oncology. 2025; 15: 1605568. https://doi.org/10.3389/fonc.2025.1605568.

[25] Jakobsen JK. Sentinel Node Methods in Penile Cancer - a Historical Perspective on Development of Modern Concepts. Seminars in Nuclear Medicine. 2022; 52: 486–497. https://doi.org/10.1053/j.semnuclmed.2021.11.010.

[26] Hollis R, Weber KT, Parikh S, Kobritz M, Gurien S, Greenwald ML. Correlation between lymph node size on pathology

and metastatic disease in right-sided colon cancer: A retrospective review. Surgical Oncology. 2023; 46: 101872. https://doi.org/10.1016/j.suronc.2022.101872.

[27] Sun K, Wang J, Wang B, Wang Y, Lu S, Jiang Z, *et al*. Non-invasive multi-phase CT artificial intelligence for predicting pre-treatment enlarged lymph node status in colorectal cancer: a prospective validation study. European Radiology. 2025; 35: 7845–7855. https://doi.org/10.1007/s00330-025-11723-w.

[28] Apollonio B, Spada F, Petrov N, Cozzetto D, Papazoglou D, Jarvis P, *et al*. Tumor-activated lymph node fibroblasts suppress T cell function in diffuse large B cell lymphoma. The Journal of Clinical Investigation. 2023; 133: e166070. https://doi.org/10.1172/JCI166070.

[29] Shome M, Gao W, Engelbrektson A, Song L, Williams S, Murugan V, *et al*. Comparative Microbiomics Analysis of Antimicrobial Antibody Response between Patients with Lung Cancer and Control Subjects with Benign Pulmonary Nodules. Cancer Epidemiology, Biomarkers & Prevention. 2023; 32: 496–504. https://doi.org/10.1158/1055-9965.EPI-22-0384.

[30] Demicheli R, Dillekås H, Straume O, Biganzoli E. Distant metastasis dynamics following subsequent surgeries after primary breast cancer removal. Breast Cancer Research. 2019; 21: 57. https://doi.org/10.1186/s13058-019-1139-7.

[31] Pu T, Liu Y, Pei Y, Peng J, Wang Z, Du M, *et al*. NIR-II Fluorescence Imaging for the Detection and Resection of Cancerous Foci and Lymph Nodes in Early-Stage Orthotopic and Advanced-Stage Metastatic Ovarian Cancer Models. ACS Applied Materials & Interfaces. 2023; 15: 32226–32239. https://doi.org/10.1021/acsami.3c04949.

[32] Wang J, Li T, Ma L, Liu G, Wang G, Kang J. NDRG2 inhibition facilitates angiogenesis of hepatocellular carcinoma. Open Medicine. 2021; 16: 742–748. https://doi.org/10.1515/med-2021-0268.

[33] Guo Z, Jing X, Sun X, Sun S, Yang Y, Cao Y. Tumor angiogenesis and anti-angiogenic therapy. Chinese Medical Journal. 2024; 137: 2043–2051. https://doi.org/10.1097/CM9.0000000000003231.

[34] Lanitis E, Irving M, Coukos G. Tumour-associated vasculature in T cell homing and immunity: opportunities for cancer therapy. Nature Reviews. Immunology. 2025; 25: 831–846. https://doi.org/10.1038/s41577-025-01187-w.

[35] Alves Rosa J, Calle-Toro JS, Kidd M, Andronikou S. Normal head and neck lymph nodes in the paediatric population. Clinical Radiology. 2021; 76: 315.e1–315.e7. https://doi.org/10.1016/j.crad.2020.12.020.

[36] Yang Z, Zhang X, Bai X, Xi X, Liu W, Zhong W. Anti-angiogenesis in colorectal cancer therapy. Cancer Science. 2024; 115: 734–751. https://doi.org/10.1111/cas.16063.

[37] Lin Q, Choyke PL, Sato N. Visualizing vasculature and its response to therapy in the tumor microenvironment. Theranostics. 2023; 13: 5223–5246. https://doi.org/10.7150/thno.84947.

[38] Li ZM, Zhou W, Feng L, Zhang HY, Chen WB. Predictive value of preoperative CT enhancement rate and CT perfusion parameters in colorectal cancer. BMC Gastroenterol. 2024; 24: 176. https://doi.org/10.1186/s12876-024-03257-0.

[39] Wu WK, Patel K, Padmanabhan C, Idrees K. Hepatocellular carcinoma presenting as an extrahepatic mass: A case report and review of literature. World Journal of Gastrointestinal Oncology. 2024; 16: 2241–2252. https://doi.org/10.4251/wjgo.v16.i5.2241.

[40] von Renesse J, Lin MC, Ho PC. Tumor-draining lymph nodes - friend or foe during immune checkpoint therapy? Trends in Cancer. 2025; 11: 676–690. https://doi.org/10.1016/j.trecan.2025.04.008.

[41] Kawagoe T, Ikeda G, Oshiro Y, Kaneko K, Iwakiri K. A Proposed New Clinical Classification of Metastatic Gastric Cancer: Pyloric and Antral Gastric Cancer. Journal of Nippon Medical School. 2022; 89: 176–183. https://doi.org/10.1272/jnms.JNMS.2022_89-212.

[42] Shimada Y, Matsumoto A, Abe K, Tajima Y, Nakano M, Arizumi T, *et al*. Primary adenocarcinoma arising from rectal implantation cyst after low anterior resection for rectal cancer 31 years previously. Clinical Journal of Gastroenterology. 2024; 17: 899–903. https://doi.org/10.1007/s12328-024-02002-0.

[43] Kido H, Kato S, Funahashi K, Shibuya K, Sasaki Y, Urita Y, *et al*. The metabolic parameters based on volume in PET/CT are associated with clinicopathological N stage of colorectal cancer and can predict prognosis. EJNMMI Research. 2021; 11: 87. https://doi.org/10.1186/s13550-021-00831-5.